Differences in conformational dynamics of [Pt₃(HPTAB)]⁶⁺–DNA adducts with various cross-linking modes

Yanyan Zhu, Yan Wang* and Guangju Chen*

College of Chemistry, Beijing Normal University, Beijing 100875, P. R. China

ABSTRACT

We present here molecular dynamics simulations and DNA conformational dynamics for a series of trinuclear platinum [Pt₃(HPTAB)]⁶⁺-DNA adducts [HPTAB = *N,N,N′,N′,N′′,N′′*-hexakis (2-pyridyl-methyl)-1,3,5-*tris*(aminomethyl) benzene], including three types of bifunctional crosslinks and four types of trifunctional crosslinks. Our simulation results reveal that binding of the trinuclear platinum compound to a DNA duplex induces the duplex unwinding in the vicinity of the platination sites, and causes the DNA to bend toward the major groove. As a consequence, this produces a DNA molecule whose minor groove is more widened and shallow compared to that of an undamaged bare-DNA molecule. Notably, for trifunctional cross-links, we have observed extensive DNA conformational distortions, which is rarely seen for normal platinum–DNA adducts. Our findings, in this study, thus provide further support for the idea that platinum compounds with trifunctional intra-strand or long-range-inter-strand cross-linking modes can generate larger DNA conformational distortions than other types of cross-linking modes.

INTRODUCTION

Cisplatin (CP) and carboplatin are extensively used in the treatments of many severe cancers, such as testicular, ovarian, bladder, head and neck, cervical and non-small cell lung cancers (1–5). However, many types of tumors have been reported to become resistant to these platinum-based chemotherapeutic agents (6–8). The resistance of tumors to these compounds is primarily attributed to the recognition and removal of Pt(II)-GG crosslinks from DNA by proteins and enzymes through the nucleotide excision repair (NER) pathway (9–11). For example, a number of damage recognition proteins and cellular proteins, especially those with high mobility group (HMG) domains, have been shown to bind specifically to Pt–GG intra-strand DNA adducts (12–18). Moreover, some thiol- and selenium-containing proteins, such as selenoenzyme thioredoxin reductase (TrxR) efficiently inhibited by CP and oxaliplatin, are also major targets for the platinum compounds within cells (19–22). To overcome this problem, one promising approach is to design platinum(II) complexes that can form different types of DNA lesions other than the typical Pt(II)–GG crosslinks (1-4). Aliphatic polyamine-bridged polynuclear platinum compounds represent such a novel class of platinum-based antitumor agents. Since these complexes are capable of forming long range intra- and inter-strand crosslinks between Pt–drug and DNA (23,24), the DNA adducts formed by these compounds are different from those by CP. Using these molecules may thus help circumvent the CP resistance problem mentioned above. The cytotoxic response to platinum anticancer agents is thought to be primarily due to the formation of the intra-strand Pt–GG adducts (6,25–29). Because proteins primarily interact with the minor groove of DNA (30), it is hypothesized that the ability of proteins to distinguish between CP–GG and other cross-linking adducts probably results from subtle differences in conformations or conformational dynamics in the Pt–DNA cross-linking modes rather than from the physical interactions of the proteins with the carrier ligands of the adducts in the major groove (1,3,4,31). Therefore, gaining insights into conformational dynamics may help better understand the cytotoxic response to platinum drugs–DNA adducts.

A representative class of the polyamine-bridged polynuclear platinum compounds which can form intra-/inter-strand DNA adducts and display high efficient antitumor activity, has attracted considerable attention in recent years (2,32–34). For instance, a well-known trinuclear platinum compound, BBR3464, in which two monofunctional Pt centers are bridged by linear aliphatic linkers and the third Pt(II) one is coordinately saturated, has entered Phase II clinical trials (35–37). These polynuclear

*To whom correspondence should be addressed. Tel: +86 10 58805424; Fax: +86 10 58802075; Email: gjchen@bnu.edu.cn
Correspondence may also be addressed to Yan Wang. Tel: +86 10 58805247; Fax: +86 10 58802075; Email: wangy@bnu.edu.cn
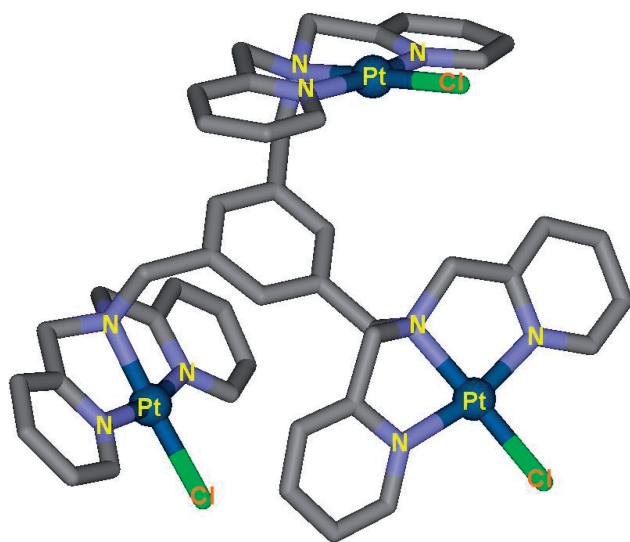
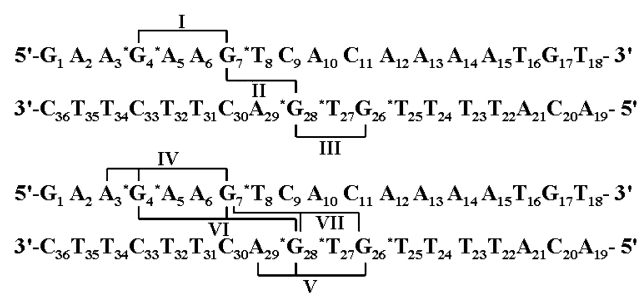**Chart 1.** X-ray structure of the trinuclear platinum compound (39).

Chart 2. The 18-mer DNA sequence and seven Pt–DNA cross-linking modes studied in this work along with their assigned names (39). Three types of bifunctional crosslinks: **I**: 4,7-DNA; **II**: 26,28-DNA; **III**: 7,28-DNA Four types of trifunctional crosslinks: **IV**: 3,4,7-DNA; **V**: 26,28,29-DNA; **VI**: 4,7,28-DNA; **VII**: 7,28,26-DNA.

compounds represent a completely new paradigm for platinum-based anticancer complexes, and appear to offer great potential as new anticancer agents (1,34). In addition, a class of chelated polynuclear platinum compounds has also been designed and exhibits interesting cytotoxicity against human and mouse cell lines (27). More recently, a trinuclear platinum compound $[Pt_3(HPTAB)Cl_3]^{3+}$ (shown in Chart 1) reported by Guo's group, in which the Pt(II) centers are bridged by bulky aromatic linkers, not only shows greater stability but also produces significantly higher cytotoxicity than CP (38). Binding experiments of this compound with the 18-mer duplex 5′-d(GAAGAAGT CACAAAATGT)-3′·5′- d(ACATTTTGTGACTTCTTC)-3′ (shown in Chart 2) suggest that the duplex offers several potential reactive sites for the Pt(II) compound to form intra-/inter-strand bi/trifunctional crosslinks, which represent long-range DNA–Pt(II) drug adducts (39). These trinuclear platinum compounds carry unique structural properties for DNA binding and can display different DNA-adduct profiles (9,40). Long range intra- and inter-strand cross-linking adducts between DNA and Pt(II)-based drugs differ greatly from the CP–GG adducts conformation-wise (2,32,41). Due to the important role of these adducts in promoting the antitumor activity, long range intra- and inter-strand crosslinks between DNA and Pt(II)-based drugs have become the focal point of interest in the studies of platinum-based anticancer drugs (1,2,32).

Understanding the structural details of DNA bound by the polynuclear platinum compounds may help us delineate the features that are responsible for the remarkable potency of these platinum drugs (1). However, knowledge of the precise interaction mechanisms of platinum anticancer drugs with DNA at the molecular level is still scarce (5). Especially, conformations and structures of Pt(II) compound–DNA adducts with long range cross-linking modes produced by trinuclear platinum compounds such as $[Pt_3(HPTAB)Cl_3]^{3+}$, are not yet clear (9,40) despite the

existence of experimental data for several bifunctional and trifunctional cross-linking modes (39). In the present work, we used molecular dynamics simulations to study the conformational properties of the $[Pt_3(HPTAB)]^{6+}$ –DNA adducts. Seven different adduct models with bi/trifunctional and intra-/inter-strand crosslinks were investigated. DNA conformational dynamics calculations were performed to examine the differences between bifunctional and trifunctional cross-linking modes and between intra- and inter-strand cross-linking modes in these Pt(II)–DNA adducts.

MODELS AND METHODS

Starting structures

Seven cross-linking adducts formed between the trinuclear platinum compound, $[Pt_3(HPTAB)Cl_3]^{3+}$, and the 18-mer duplex DNA, 5′-d(GAAGAAGTCACAAAATGT)-3′·5′-d(ACATTTTGTGACTTCTTC)-3′ that was chosen from breast/ovarian cancer-susceptibility genes BRCA1 (Genbank #U14680) (42), are presented in Chart 2, i.e. three types of bifunctional cross-linking modes: intra-1,4-GG crosslink I mode (assigned as 4,7-DNA), intra-1,3-GG crosslink II mode (assigned as 26,28-DNA) and inter-1,3′-GG crosslink III mode (assigned as 7,28-DNA); and four types of trifunctional cross-linking modes: intra-1,2,5-AGG crosslink IV mode (assigned as 3,4,7-DNA), intra-1,3,4-GGG crosslink V mode (assigned as 26,28, 29-DNA), intra-1,4,6′-GGG crosslink VI mode (assigned as 4,7,28-DNA) and intra-1,3′,5′-GGG crosslink VII mode (assigned as 7,28,26-DNA). The connection points of these adduct models were examined previously by denaturing polyacrylamide gels and MALDI–TOF MS analysis (39). However, no crystal structures for these adducts have been solved so far. From previous studies, it has been predicted that the three Pt center atoms possibly bind to the N7 atoms of G/A bases of DNA (43). The initial coordinates of seven Pt(II)–DNA adducts used in our simulations were generated by docking platinum complex in the major groove of DNA. Since several different orientations of Pt compound coordinating with the major groove of DNA for each binding adduct were chosen as the starting structures for our molecular dynamics

(MD) simulations, this provides a good test of whether our MD simulations are capable of driving significantly distinct starting structures to a non-distinguishable one when simulations reach equilibrium. Bump-checking was turned on to ensure that no overlapping atoms were produced during the docking process. To compare the differences between the DNA adduct conformations and an undamaged DNA molecule, a bare-DNA (B-DNA) molecule simulation was also performed, in which an idealized B-DNA was used as a starting structure for the simulation. Given that each strand of DNA has some phosphate groups, Na^+ counterions were added to each system to achieve electroneutrality. The systems were explicitly solvated using the TIP3P water potential inside a box large enough to ensure the solvent shell extended to 10 Å in all directions.

Force field parameter preparation

The atom types for the studied platinum compound, except for the platinum atoms, were generated using the ANTECHAMBER module in the AMBER9 program. The electrostatic potentials of the platinum compound used for RESP charge calculations were calculated at the HF/6-31G** + LanL2DZ (44–46) level of theory using the Gaussian03 program (47). RESP charges of the platinum compound were derived by the RESP program based on the calculated electrostatic potentials. The force field parameters of the platinum compound related to platinum atoms were referenced from previous works (48–50). Other force field parameters of the platinum compound were generated from the gaff force field in the AMBER9 program.

Molecular dynamics simulations

All MD simulations were carried out using the AMBER9 package (51) and the parm99 force field (10,52) of AMBER together with the parmbsc0 refinement (48) and gaff (53) force field parameters. The protocol for all MD simulations is as follows: (1) All systems were submitted to energy minimization to remove unfavorable contacts. Four cycles of minimizations were performed with 2500 steps in each minimization with harmonic restraints ranging from $100\,kcal\,mol^{-1}\,Å^{-2}$, $25\,kcal\,mol^{-1}\,Å^{-2}$ to $10\,kcal\,mol^{-1}\,Å^{-2}$ on DNA and the platinum compound positions. Finally, 5000 steps of unrestrained minimization were carried out before the heating process. The cutoff distance used for non-bonded interactions was 10 Å. The SHAKE algorithm (54) was used to restrain the bonds containing hydrogen. (2) Each energy-minimized structure was heated over 120 ps from 0 to 300 K (with a temperature coupling of 0.2 ps) in a constant volume, while the positions of DNA and the platinum compound were restrained with a small value of $10\,kcal\,mol^{-1}\,Å^{-2}$. (3) The unrestrained equilibration of 200 ps with constant pressure and constant temperature conditions was carried out before a trajectory was generated for a further production simulation. The temperature and pressure were allowed to fluctuate around 300 K and 1 bar respectively with a corresponding coupling of 0.2 ps. For each simulation, an integration step of 2 fs was used. (4) Production runs of 20 ns were carried out by following the same protocol. A time point of 200 ps after thermal equilibration in each simulation was selected as a starting point for data collection. During the production run, 10 000 structures from each simulation were saved for post-processing by uniformly sampling the trajectory (5). Finally, simulated annealing was performed for each system by allowing the system to cool from 300 to 0 K during the course of 1 ns simulation.

### DNA helical parameter analysis of trajectories

The PTRAJ module of the AMBER9 program was used to extract production conformations. These extracted snapshots were saved in the Protein Data Bank (PDB) format. Each nucleotide type was converted from the AMBER format to PDB format, and the resulting snapshots were submitted to the CURVES program (55). The following CURVES parameters were extracted, i.e. global base-pair helical parameters: buckle and propeller; and global inter base-pair step helical parameters: shift, slide, roll and twist. Percentage occupancy distributions of the DNA helical parameters were calculated by normalizing the frequency distributions to 100%.

The overall bend, tilt and roll angles of DNA for the average structures of these adducts were calculated from the CURVES output using MadBend (http://www.biomath.nyu.edu/index/software/Madbend/index.html) developed by Strahs and Schlick (56). This method evaluates the DNA curvature by summing the projected components of local base-pair step tilt and roll angles after adjusting the helical twist. Bends in the helical axis defined by a negative roll angle indicate bending toward the minor groove, while bends defined by a positive roll angle correspond to bending toward the major groove (56).

RESULTS AND DISCUSSION

General characterization of the MD simulations

First, the root-mean-square deviation (RMSD) values of all backbone atoms referenced to the corresponding starting structures over all seven trajectories were examined to determine if each system had attained equilibrium. It is often considered that small RMSD values of a simulation indicate a stable state of a platinum–DNA (Pt–DNA) adduct. Plots of RMSDs of seven system simulations over time are shown in Figure 1. It can be seen from Figure 1 that each Pt–DNA adduct reached equilibrium after 1 ns, and their energies were found to be stable during the remainder of each simulation. Therefore, a time of 1 ns after thermal warm-up was selected as a starting point for data analysis of each simulation. The trajectory analysis for each system involves extracting the equilibrated conformations between 1 ns and 20 ns of simulation time, recording 9500 snapshots at every 2 ps time-interval of each trajectory.
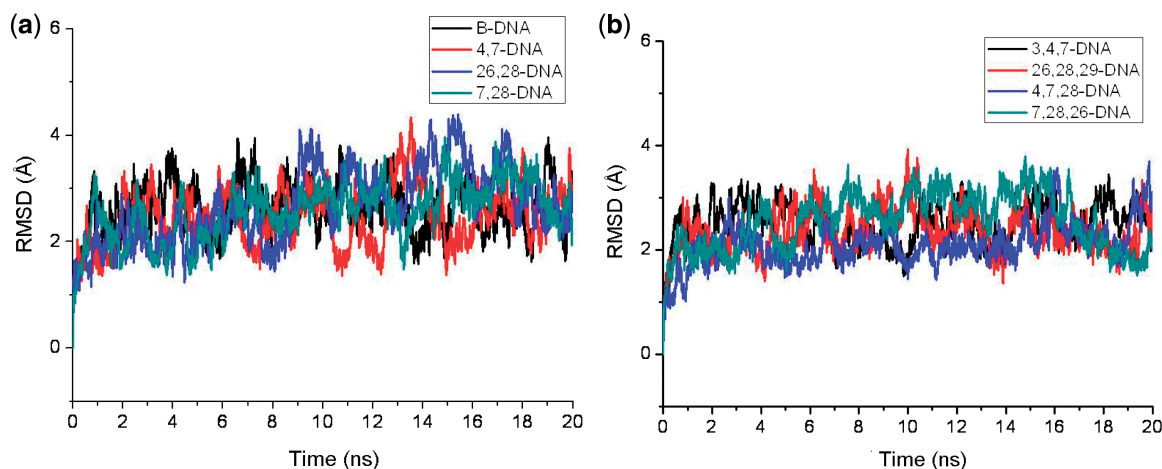
Figure 1. The RMSD values of all backbone atoms for (**a**) the simulations of B-DNA and bifunctional crosslinks and (**b**) the simulations of trifunctional crosslinks with respect to the corresponding starting structures.

Principal component analysis of major conformational dynamics

Principal component analysis (PCA) a linear analysis technique, can be used to find the most efficient representation (in the least-squares sense) of a data set in a few dimensions (57). By calculating the eigenvectors from the covariance matrix of a simulation and then filtering the trajectories along each of the different eigenvectors, it is possible to identify the dominant motions observed during a simulation by visual inspection. A large portion of the overall fluctuations of macromolecules can often be accounted for by a few low-frequency eigenvectors with large eigenvalues. As PCA reduces the dimensionality of the trajectory data, using only the first several principal components we can extract important dynamical features describing collective and overall motions of the system (58–61). To identify the dominant DNA motions in the studied Pt–DNA adducts, PCA applied to the backbone atoms in the seven Pt–DNA adducts results in the first three principal components (PC1, PC2 and PC3), which describe about 80% of all the motion modes (Table 1). These first three components of conformational motions roughly correspond to a superposition of bending, unwinding and twisting motions.

Visual analyses of the trajectories of average DNA structures in the simulation support the PCA dominant motions described above. The overall centroid structures of seven adducts from 1 ns to 20 ns simulations are shown in Figure 2. It can be seen from Figure 2 that the DNA conformation of each Pt–DNA crosslink including the bending motion, unwinding extent and twisting degree, shows obvious differences from the undamaged B-DNA conformation. Especially, (i) the bending motion feature is clearly present for all adducts; (ii) the unwinding motions of the trifunctional cross-linking modes in the vicinity of the platination sites lead to a large change to the DNA groove conformation with respect to the undamaged B-DNA molecule, which makes it more difficult for DNA repair as well as gene transcription, thus improving the CP drug resistance; (iii) at the same time, the twisting motions cause the DNA structures in the adducts to have

Table 1. Percentages of occupancy times of the first three principal components during the simulations of the studied Pt–DNA adducts

Adducts	PC1	PC2	PC3	PCs
4,7-DNA	63.59	21.90	9.57	95.07
26,28-DNA	48.04	23.80	9.07	80.91
7,28-DNA	68.29	17.23	6.65	92.17
3,4,7-DNA	71.06	9.55	7.61	88.22
26,28,29-DNA	64.67	14.89	8.19	87.75
4,7,28-DNA	74.39	15.25	4.92	94.56
7,28,26-DNA	71.61	13.58	7.36	92.55

PCs represents sum of PC1, PC2 and PC3.

a significant distortion from a canonical B-DNA, including some bases moving away from the groove; (iv) the first three motions take place simultaneously and are irreversible.

Hydrogen bond analysis

To estimate the stability of the DNA duplex, the occupancy of all possible hydrogen bonds for each adduct was measured by calculating the percentage of time during the simulation that the hydrogen bonds exist. The obtained data for the hydrogen bond occupancy are shown in Figure 3. When compared to B-DNA, it can be seen from Figure 3a for bifunctional crosslinks that the hydrogen bond occupancy of base pairs in the vicinity of the platination sites on the 5′ side of the adducts shows a significant decrease, whereas the base pairs on the 3′ side of the adducts are almost completely intact. Apparently, for trifunctional crosslinks, as shown in Figure 3b, distinct differences for hydrogen bond occupancy occur in the vicinity of the platination sites, which has hardly any hydrogen bond occupancy for several consecutive base pairs in these adducts, such as 5, 3 and 4 bp, respectively, for 3,4,7-DNA, 26,28,29-DNA and 7,28,26-DNA adducts. This is a rare phenomenon for Pt–DNA adducts, which can result in real damage to the original DNA structure. Comparing the modes of different types of cross-links
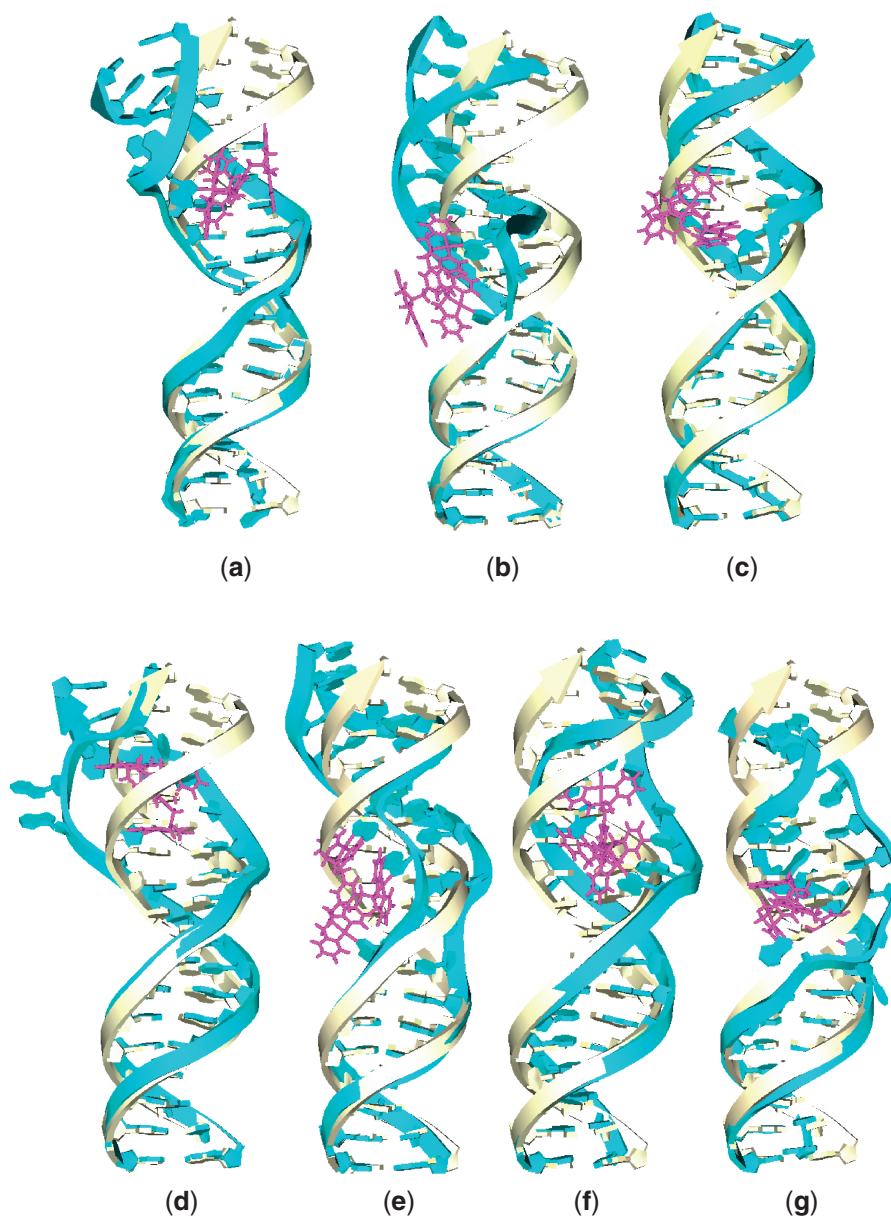
Figure 2. The average centroid structures of seven adducts (the double-strand DNA backbones (green) with an arrow from 5′- to 3′-side in ribbon, and the studied platinum compounds in stick (pink)) along with an undamaged B-DNA (light yellow). (**a**) 4,7-DNA, (**b**) 26,28-DNA, (**c**) 7,28-DNA, (**d**) 3,4,7-DNA, (**e**) 26,28,29-DNA, (**f**) 4,7,28-DNA and (**g**) 7,28,26-DNA.

shows that the distortions of the DNA duplexes influenced by trifunctional crosslinks are greater than those caused by bifunctional crosslinks. Similar observations for intra-/inter-strand cross-linking modes reveal that the distortions of DNA conformations induced by intra-strand crosslinks are greater than those caused by inter-strand ones.

Two types of hydrogen bonds with significantly high occupancy between the platinum carrier ligand and the DNA molecule were identified and are shown in Figure 4. One occurs between the aromatic carbon hydrogen atoms of the platinum compound and the oxygen/nitrogen atoms of the bases at or near the platination sites. The other occurs between the acyclic carbon hydrogen atoms of the platinum compound and the oxygen/

nitrogen atoms of the bases at or near the platination sites. The occupancy and type of each of these hydrogen bond combinations are summarized in Table 2. For bifunctional crosslinks, Table 2 shows that the adducts spend <10% of their time in conformations that allow for the hydrogen bond formation, as shown in Figure 4a and b for the 4,7-DNA and 7,28-DNA adducts, respectively. However, the trifunctional adducts 3,4,7-DNA and 4,7,28-DNA with longer spans spend much more occupancy time than the trifunctional adducts 26,28,29-DNA and 7,28,26-DNA with shorter spans. Specifically, the 3,4,7-DNA and 4,7,28-DNA adducts spend 60% and 83% of their time in conformations that allow for the formation of the hydrogen bonds between the compound
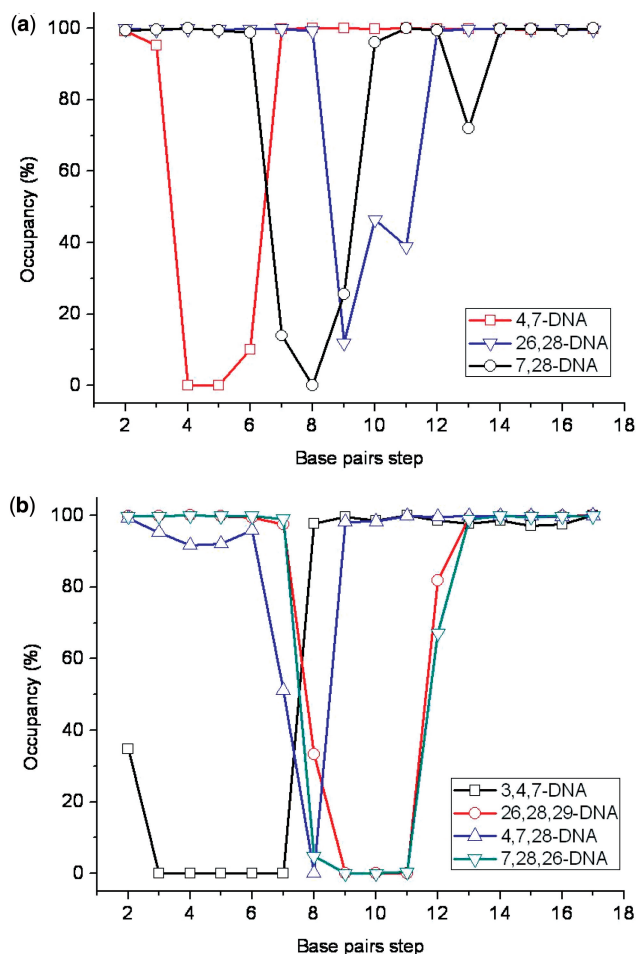
Figure 3. Hydrogen bond occupancies of base pairs along with base-pair steps for each adduct: (**a**) for 4,7-DNA (square), 26,28-DNA (down-triangle), 7,28-DNA (circle); (**b**) 3,4,7-DNA (square), 26,28, 29-DNA (circle), 4,7,28-DNA (up-triangle) and 7,28,26-DNA (down-triangle).

carbon H atom and the N3/O2 atom of the C30/T31/T32 base, and between the compound carbon H atom and the N7/O6 atom of the G28/A29 base, as shown in Figures 4c and d for the 3,4,7-DNA and 4,7,28-DNA adducts, respectively. However, the 26,28,29-DNA adduct spends only 15.53% of its time in a conformation that allows for the formation of the hydrogen bonds between the compound carbon H atom and the N1/N3 atom of the A29 base. Thus, for the 3,4,7-DNA and 4,7,28-DNA adducts the occupancies of hydrogen bonds are greater than those for other adducts, suggesting that the long-range trifunctional adducts make the distorted DNA conformation more stable. These observations demonstrate that the long-range trifunctional crosslinks form hydrogen bonds which facilitate the DNA conformational distortion.

DNA conformational dynamics

To determine the effect of the studied seven Pt–DNA adducts on the conformational dynamics of DNA, the frequency distributions (fraction of the time spent in each conformation) from the trajectories of seven adducts

and an undamaged DNA simulations were calculated using the CURVES program (55). To account for the distortion of the whole DNA backbone by the platinum compound, the overall bend, tilt and roll angles of the DNA average structures for the studied adducts were calculated from the CURVES output using the MadBend program (56).

Overall helical parameters of DNA conformations. Table 3 gives the values of overall bend, tilt and roll angles for the DNA conformations of the studied adducts. It can be seen from Table 3 that the measured degrees of overall DNA bend, tilt and roll angles for the bound-DNA backbone conformation of each adduct are certainly different from those for the undamaged B-DNA molecule. Namely, the average deviation percentages of helical angles with respect to the undamaged B-DNA molecule are 134.3% (154.6% for bend; 200.4% for tilt; 48.0% for roll) and 180.8% (199.9% for bend; 230.7% for tilt; 111.8% for roll) for the bifunctional and trifunctional adducts, respectively. As expected, the distorted degrees of bound DNA molecules for trifunctional adducts are larger than those for the bifunctional ones. In other words, the trifunctional cross-linking modes can cause a greater DNA helical conformation distortion than the bifunctional ones, which is consistent with previous studies (41). Interestingly, the bend angles toward the major groove were observed for most of the adducts studied, which suggests that there is great stability of the bound DNA conformations for this orientation, except for the 7,28,26-DNA adduct with the bend angle toward the minor groove.

Base pair and base-pair step helical parameters of DNA conformations. To address the effect of different cross-linking modes on the DNA conformational dynamics, the frequency distributions of the DNA helical parameters at the base pair near the Pt–DNA connecting sites for all types of Pt–DNA adducts including the undamaged B-DNA were analyzed for statistical significance by the Kologorov–Smirnov test. Figures 5 and 6 show the distributions for the bifunctional and trifunctional cross-linking modes, respectively. The Kologorov–Smirnov test determines how significantly these distributions differ from each other without making any assumptions regarding the distribution of data (non-parametric and distribution-free). The DNA helical parameters include the base-pair helical parameters of propeller and buckle, and the base-pair step helical parameters of shift, slide, roll and twist. Those helical parameters can be used to measure the extent of a DNA structure deviation from its canonical reference state. As expected, the positions with all parameter changes fall in the vicinity of the platination sites.

Cases in which the frequency distributions of the DNA helical parameters were significantly different from the undamaged B-DNA for three types of the bifunctional cross-linking Pt–DNA adducts are shown in Figure 5. To compare the three bifunctional adducts to the undamaged B-DNA, there were several distinct differences identified. Namely, the differences include (1) for the 4,7-DNA adduct, the propeller twist/buckle for the G4·C33 and G7·C30 base pairs, shift/slide/roll/twist for
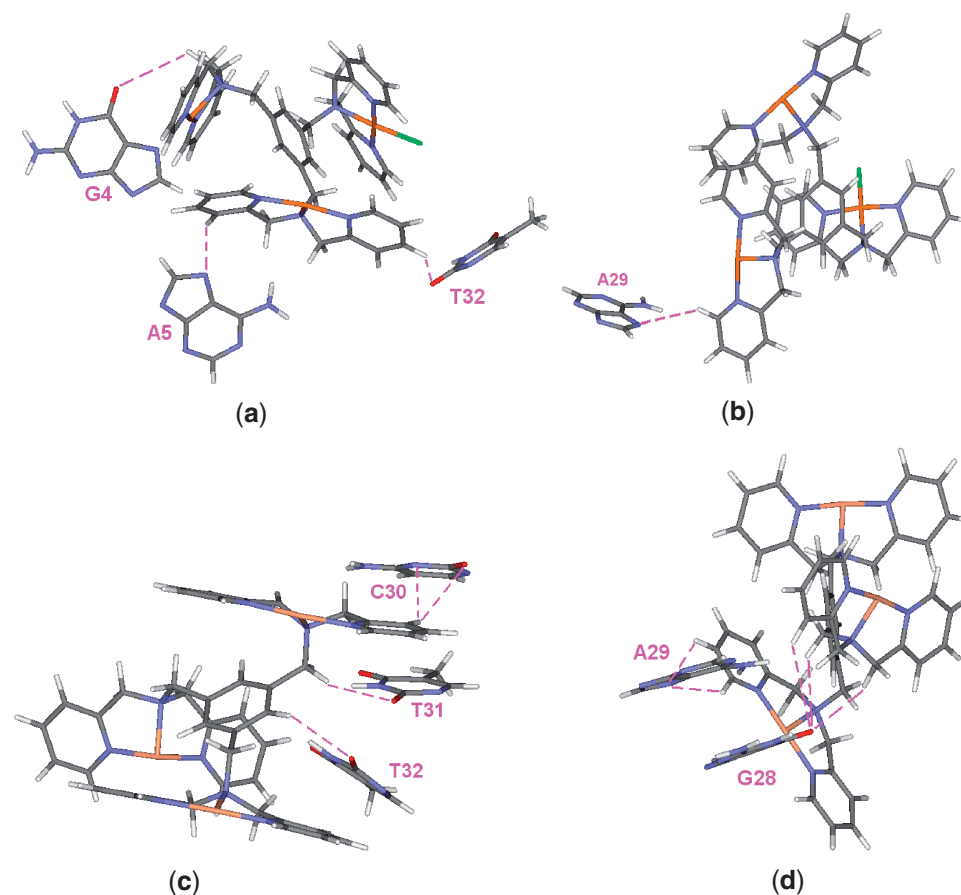
Figure 4. Hydrogen bonds between platinum ligands and DNA: the bases in DNA and the platinum compound in tube, carbon atoms in gray, nitrogen atoms in blue, oxygen atoms in red and hydrogen atoms in white; (**a**) 4,7-DNA, (**b**) 26,28-DNA, (**c**) 3,4,7-DNA and (**d**) 4,7,28-DNA.

Table 2. Occupancies of hydrogen bonds between carbon hydrogen atoms of the platinum compound (electron acceptor) and near bases on the DNA (electron donor)

Adducts	Electron donor	Electron acceptor	Occupancy (%)
4,7-DNA	G4/O6	H-C_c^a	8.60
	A5/N7	H-C_a^b	5.95
	T32/O2	H-C_a^b	1.28
26,28-DNA	A29/N7	H-C_a^b	8.53
7,28-DNA	T8/N3	H-C_a^b	4.45
3,4,7-DNA	T32/O2	H-C_a^b	60.60
	T31/N3	H-C_c^a	38.43
	T8/O2	H-C_a^b	25.84
	C30/N3	H-C_a^b	17.73
	C30/O2	H-C_a^b	5.26
26,28,29-DNA	G28/O6	H-C_a^b	15.53
	A29/N3	H-C_a^b	9.12
	A29/N1	H-C_a^b	7.67
4,7,28-DNA	G28/O6	H-C_c^b	83.79
	A29/N7	H-C_a^b	51.96
7,28,26-DNA	T25/O4	H-C_a^b	2.63

C_c^a: acyclic carbon atom in the linker region; C_a^b: aromatic carbon atom in the pyridyl group.

Table 3. Values of average overall bend, tilt and roll angles (°) for the DNA conformations of the studied adducts and undamaged B-DNA

| Adducts	Bend	Tilt	Roll
B-DNA	21.8	10.3	18.4
4,7-DNA	52.1	42.2	26.7
26,28-DNA	57.2	56.5	6.8
7,28-DNA	43.9	39.2	11.8
3,4,7-DNA	77.4	59.2	46.7
26,28,29-DNA	39.9	5.1	41.2
4,7,28-DNA	72.7	62.4	35.7
7,28,26-DNA	71.6	55.3	−32.3

step, and shift/twist for the G28·A29 base-pair step; (3) for the 7,28-DNA adduct, buckle for the C9·G28 base pair, shift/twist for the G7·T8/G28·A29 base-pair step. These differences indicate that the conformational dynamics profile of B-DNA is altered by the platinum adducts. Especially, the profiles of frequency distributions of the base-pair helical and base-pair step parameters for the 4,7-DNA adduct show extensively flat curves far from the location of the undamaged B-DNA, which implies that the long span of platinum adducts allows for the large conformational flexibility of DNA backbones. In addition, for the intra-strand 4,7-DNA and

the G4·A5 base-pair step, and shift/twist for the G7·T8 base-pair step; (2) for the 26,28-DNA adduct, the propeller twist for the C9·G28 base pair, buckle for the C11·G26 base pair, shift/slide/roll/twist for the G26·T27 base-pair
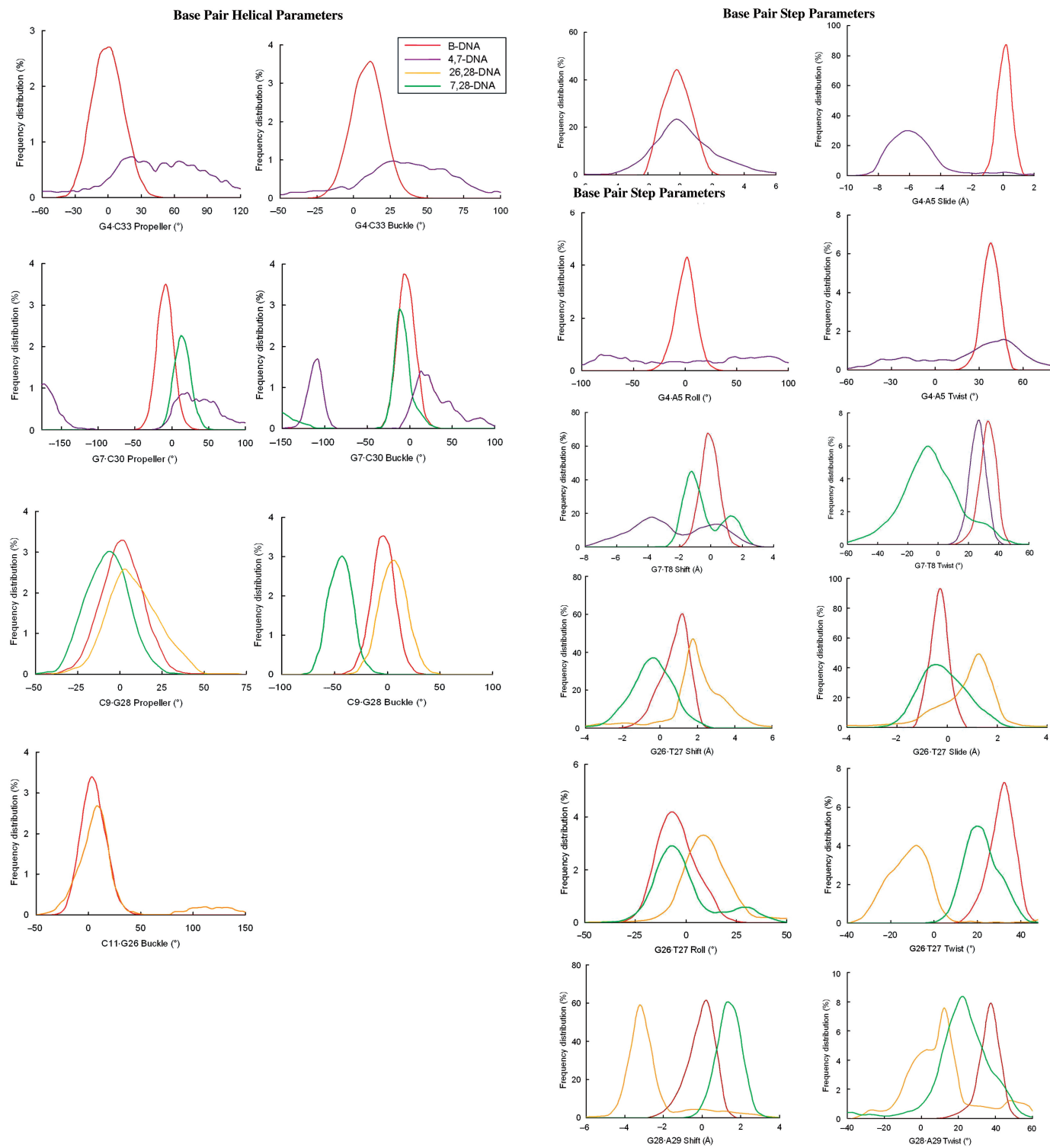
Figure 5. Selected frequency distributions of the representative DNA duplex helical parameters for the central binding base pairs for the bifunctional crosslinks.
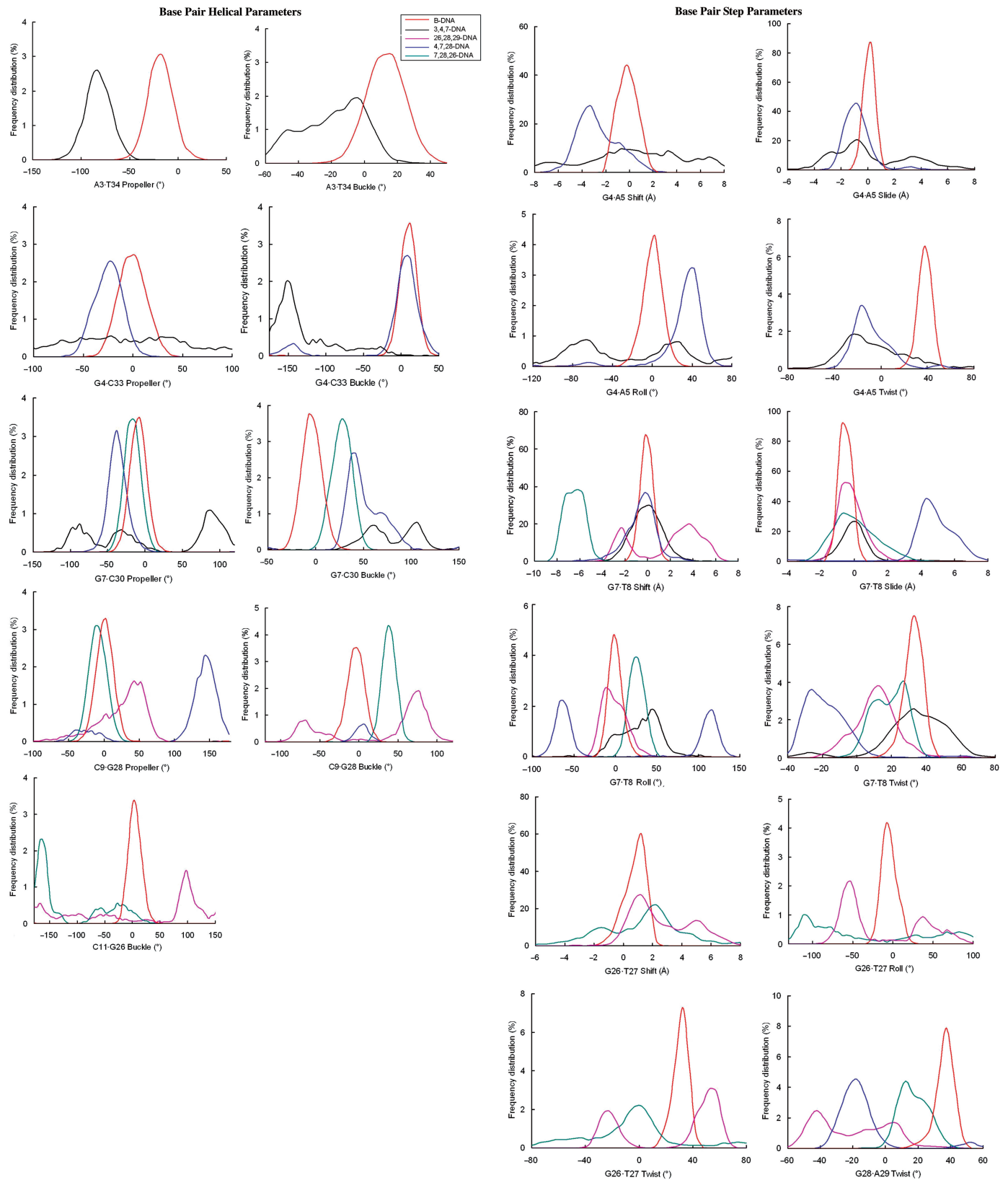
Figure 6. Selected frequency distributions of the representative DNA duplex helical parameters for the central binding base pairs for the trifunctional crosslinks.

26,28-DNA adducts, the differences between their DNA helical parameters and those of an undamaged B-DNA are more striking than those for the inter-strand 7,28-DNA adduct, which agrees with previous studies (62–64).

The frequency distributions of DNA helical parameters for four types of the trifunctional cross-linking Pt–DNA adducts are shown in Figure 6 along with the distribution patterns of the undamaged B-DNA. Between the four trifunctional Pt–DNA adducts and the undamaged B-DNA, there are still several distinct differences identified. Namely, the differences include (i) for the 3,4,7-DNA adduct, the propeller twist/buckle for the A3·T34, G4·C33 and G7·C30 base pairs, shift/slide/roll/twist for the G4·A5 base-pair step, and roll for the G7·T8 base-pair step; (ii) for the 26,28,29-DNA adduct, the propeller twist/buckle for the C9·G28 base pair, buckle for the C11·G26 base pair, shift/roll/twist for the G26·T27 base-pair step, and twist for the G28·A29 base-pair step; (iii) for the 4,7,28-DNA adduct, the propeller twist for the G4·C33 base pair, buckle for the G7·C30 base pair, shift/roll/twist for the G4·A5 base-pair step, slide/roll/twist for the G7·T8 base-pair step, and twist for the G28·A29 base-pair step; (iv) for the 7,28,26-DNA adduct, propeller twist/buckle for the C9·G28 base pair, buckle for the G7·C30/ C11·G26 base pairs, shift/roll/twist for the G26·T27 base-pair step and twist for the G28·A29 base-pair step. Of note, the long-range trifunctional modes of the 1,5-intra-strand 3,4,7-DNA and 1,6′-inter-strand 4,7,28-DNA adducts show more significant differences in the frequency distributions of the DNA helical parameters from the undamaged B-DNA than the other two adducts, which is consistent with previous studies (62–66).

Next, to compare the bifunctional to trifunctional cross-link modes, it is obvious from the frequency distributions of the DNA helical parameters that the distortions of DNA conformations induced by the trifunctional cross-link modes are larger than those caused by the bifunctional ones, such as the 4,7-DNA versus the 3,4,7-DNA adduct, and the 7,28-DNA versus the 7,28,26-DNA one. When comparing the 4,7-DNA adduct to 3,4,7-DNA adduct, there are some noticeable differences. For the base-pair helical parameters, the differences were observed for the propeller twist/buckle at the G4·C33 and G7·C30 base pairs of both the 4,7-DNA and 3,4,7-DNA adducts. However, extra difference was also observed for the propeller twist/buckle at the A3·T34 base pair of the 3,4,7-DNA adduct. Such difference suggests that the trifunctional mode in the 3,4,7-DNA adduct can induce a distortion in the DNA conformation more efficiently than the bifunctional mode in the 4,7-DNA adduct. Similar observations can been made for other bifunctional 7,28-DNA and trifunctional 7,28,26-DNA adducts when comparing them with each other. These results support previous experimental and computational studies (1,2,41).

Correlation between platinum ligand hydrogen bond formation and DNA conformational dynamics

Because the formation of hydrogen bonds can influence the conformational dynamics of Pt–DNA adducts (41),

a large number of examples in which the frequency distribution of DNA helical parameters is associated with the pattern of hydrogen bond formation suggests that the conformational dynamics of many DNA helical parameters in the vicinity of the platination sites is strongly correlated with the pattern of hydrogen bond formation. For most of the DNA helical parameters shown, there is a clear difference in the distribution of the DNA helical parameters when the hydrogen bond exists at the base pairs. In the case of the 3,4,7-DNA adduct, the hydrogen bond patterns are formed (60%) at the bases C30, T31 and T32 (shown in Table 2). The frequency distributions of the DNA helical parameters associated with these hydrogen bonds are generally either almost identical (G7·C30 propeller twist/buckle) or very similar (G4·C33 propeller twist/buckle, G4·A5 shift/slide, G7·T8 roll). A similar observation for the 4,7,28-DNA adduct can also be seen in this work. These data suggest that the DNA conformations in which the hydrogen bonds are seen in the vicinity of the platination sites may represent conformational transitions. However, these patterns are not universal. For the 26,28,29-DNA adduct, there appear to be clear differences in the distributions of the DNA helical parameters from those of an undamaged B-DNA whose hydrogen bonds (15.53%) exist at only one base.

### Groove parameters and dimensions for the Pt–DNA adducts

Based on previous experimental observations on the effects of platinum drugs causing the minor groove of DNA to become widened and shallowed (39), Figure 7 compares the minor groove widths and depths from the time-averaged structures of the trifunctional Pt–DNA adducts using an undamaged B-DNA of the same length and sequence as a reference. An undamaged and canonical B-DNA has an average minor groove width of 5.87 Å and a depth of 4.64 Å (67). It is obvious from Figure 7a and b that the minor groove widths and depths change significantly at or near the vicinity of the platination sites with respect to the undamaged B-DNA. Especially, as the minor groove increases its width, the corresponding depths become shallow as compared to those from a normal B-DNA. For instance, the minor groove widths of the 3,4,7-DNA and 26,28,29-DNA adducts are widened by 106% (from 5.87 to 12.1 Å) and by 128% (from 5.87 to 13.4 Å) at the G7·C30 and C11·G26 base pairs, respectively (as shown in Figure 7a). Their corresponding minor groove depths are shoaled by 57% (from 4.64 to 2.0 Å) and by 81% (from 4.64 to 0.9 Å), respectively, compared to a normal B-DNA (as shown in Figure 7b). As expected, Figure 7c presents the properties of the widened minor groove width versus the shallow minor groove depth for the 26,28,29-DNA adduct.

Visual analyses of the conformation details at some base pairs of the 26,28,29-DNA adducts and of an undamaged B-DNA support above observations (as shown in Figure 8). In fact, the rigid linker of the trinuclear platinum compound makes it very difficult to span over more than four base pairs unless the DNA molecule has been greatly distorted. It is clearly seen from Figure 8a that the

(a)

(b)

(c)
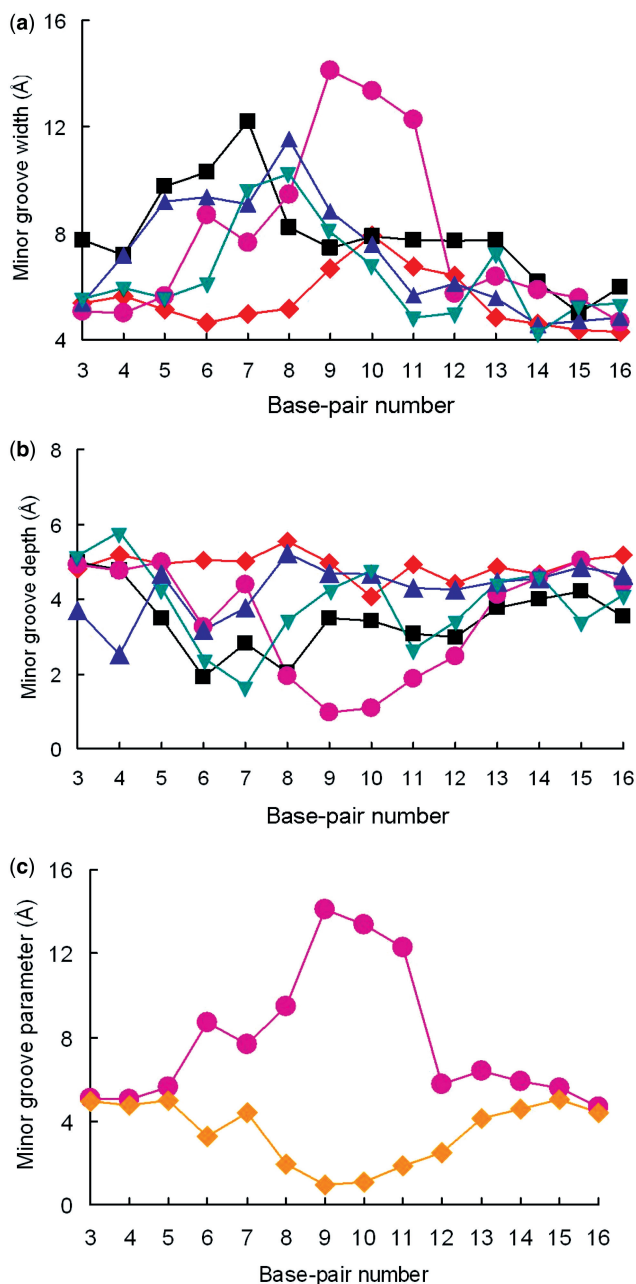
Figure 7. Minor groove widths and depths for the time-averaged structures of the DNA conformations in the four types of the trifunctional crosslinks: (**a**) and (**b**): B-DNA (red line with diamond), 3,4,7-DNA (black line with square), 26,28,29-DNA (magenta line with circle), 4,7,28-DNA (blue line with up-triangle), and 7,28,26-DNA (green line with circle); (**c**): the minor groove parameters of DNA in the 26,28,29-DNA adduct (magenta line with circle for width and light-orange line with diamond for depth).

minor groove width at the C11·G26 base pair is much wider than that of the undamaged B-DNA. Accordingly, the minor groove depth at the C11·G26 base pair shown in Figures 8b is greatly shoaled with respect to the undamaged B-DNA. In addition, it is also noticeable from Figure 8a that the adjacent bases of C9 and A10 near the platination sites have frayed from the groove of DNA and thus cause a large distortion in the DNA

(a)

(b)
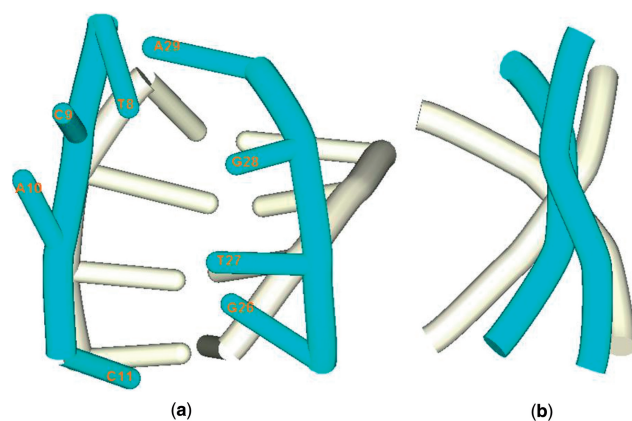
Figure 8. Conformation details of DNA base pairs in the 26,28, 29-DNA adduct along with the corresponding undamaged B-DNA base pairs: double-strand DNA backbone with light blue and the undamaged B-DNA with light yellow. (**a**) Front view of DNA backbone for 8–11 bp; (**b**) side view of DNA backbone.

conformation. However, the corresponding trajectories reveal that such distorted conformations of those trifunctional crosslink adducts are quite stable during the simulations, which might suggest that such conformational conversion is feasible and irreversible. These observations demonstrate the fact that the trifunctional intra-strand/long-span-inter-strand crosslinks induce more extensive DNA conformation damage than other types of crosslinks (24,68).

CONCLUSIONS

Molecular dynamics simulations and DNA dynamics analyses for a series of the trinuclear Pt–DNA adducts, including three types of the bifunctional crosslinks and four types of the trifunctional crosslinks, were carried out to examine the distortions inflicted on the DNA double-helical structure. In both bi- and trifunctional crosslinks, the extent of DNA conformational distortions induced by intra-strand crosslinks is greater than that caused by inter-strand crosslinks with the same span. For intra- and inter-strand crosslinks, the long-range crosslinks in Pt–DNA adducts can significantly facilitate DNA conformational distortion. Moreover, by inducing the DNA duplex unwinding in the vicinity of the platination sites and causing it to bend toward the major groove, the trifunctional crosslinks of the studied Pt–DNA adducts can produce a widened and shallow minor groove, which is a rare phenomenon for normal platinum–DNA adducts. The durable stabilities of these distorted DNA conformations on a nanosecond time scale can be advantageous in improving the antitumor activity and reducing the resistance of tumors to platinum drugs (4). Our simulation results provide useful insights for a better understanding of how a DNA conformation is affected by a platinum drug in atomic detail, and may aid in the design of other platinum-based DNA-binding agents.

ACKNOWLEDGEMENTS

REFERENCES

1. Hegmans,A., Berners-Price,S.J., Davies,M.S., Thomas,D.S., Humphreys,A.S. and Farrell,N. (2004) Long range 1,4 and 1,6-interstrand cross-links formed by a trinuclear platinum complex. Minor groove preassociation affects kinetics and mechanism of cross-link formation as well as adduct structure. *J. Am. Chem. Soc.*, **126**, 2166–2180.
2. Jung,Y. and Lippard,S.J. (2007) Direct cellular responses to platinum-induced DNA damage. *Chem. Rev.*, **107**, 1387–1407.
3. Berners-Price,S.J., Davies,M.S., Cox,J.W., Thomas,D.S. and Farrell,N. (2003) Competitive reactions of interstrand and intrastrand DNA-Pt adducts: a dinuclear-platinum complex preferentially forms a 1,4-interstrand cross-link rather than a 1,2 intrastrand cross-link on binding to a GG 14-mer duplex. *Chem. Eur. J.*, **9**, 713–725.
4. Kasparkova,J., Zehnulova,J., Farrell,N. and Brabec,V. (2002) DNA interstrand cross-links of the novel antitumor trinuclear platinum complex BBR3464. conformation, recognition by high mobility group domain proteins, and nucleotide excision repair. *J. Biol. Chem.*, **277**, 48076–48086.
5. Wong,E. and Giandomenico,C.M. (1999) Current status of platinum-based antitumor drugs. *Chem. Rev.*, **99**, 2451–2466.
6. Fuertes,M.A., Alonso,C. and Perez,J.M. (2003) Biochemical modulation of cisplatin mechanisms of action: enhancement of antitumor activity and circumvention of drug resistance. *Chem. Rev.*, **103**, 645–662.
7. Lin,X. and Howell,S.B. (2006) DNA mismatch repair and p53 function are major determinants of the rate of development of cisplatin resistance. *Mol. Cancer Ther.*, **5**, 1239–1247.
8. Clodfelter,J.E., Gentry,M.B. and Drotschmann,K. (2005) MSH2 missense mutations alter cisplatin cytotoxicity and promote cisplatin-induced genome instability. *Nucleic Acids Res.*, **33**, 3323–3330.
9. Jamieson,E.R. and Lippard,S.J. (1999) Structure, recognition, and processing of cisplatin-DNA adducts. *Chem. Rev.*, **99**, 2467–2498.
10. Duan,Y., Wu,C., Chowdhury,S., Lee,M.C., Xiong,G., Zhang,W., Yang,R., Cieplak,P., Luo,R., Lee,T. *et al.* (2003) A point-charge force field for molecular mechanics simulations of proteins based on condensed-phase quantum mechanical calculations. *J. Comput. Chem.*, **24**, 1999–2012.
11. Reed,S.H. (2005) Nucleotide excision repair in chromatin: the shape of things to come. *DNA Repair*, **4**, 909–918.
12. Wei,M., Cohen,S.M., Silverman,A.P. and Lippard,S.J. (2001) Effects of spectator ligands on the specific recognition of intrastrand platinum-DNA cross-links by high mobility group box and TATA-binding proteins. *J. Biol. Chem.*, **276**, 38774–38780.
13. Ramachandran,S., Temple,B.R., Chaney,S.G. and Dokholyan,N.V. (2009) Structural basis for the sequence-dependent effects of platinum–DNA adducts. *Nucleic Acids Res.*, **37**, 2434–2448.
14. Pil,P.M. and Lippard,S.J. (1992) Specific binding of chromosomal protein HMG1 to DNA damaged by the anticancer drug cisplatin. *Science*, **256**, 234–237.
15. Ohndorf,U.M., Whitehead,J.P., Raju,N.L. and Lippard,S.J. (1997) Binding of tsHMG, a mouse testis-specific HMG-domain protein, to cisplatin-DNA adducts. *Biochemistry*, **36**, 14807–14815.
16. Trimmer,E.E., Zamble,D.B., Lippard,S.J. and Essigmann,J.M. (1998) Human testis-determining factor SRY binds to the major DNA adduct of cisplatin and a putative target sequence with comparable affinities. *Biochemistry*, **37**, 352–362.
17. Dunham,S.U. and Lippard,S.J. (1997) DNA sequence context and protein composition modulate HMG- domain protein recognition of ciplatin-modified DNA. *Biochemistry*, **36**, 703–710.
18. Chow,C.S., Whitehead,J.P. and Lippard,S.J. (1994) HMG domain proteins induce sharp bends in cisplatin-modified DNA. *Biochemistry*, **33**, 15124–15130.
19. Lo,Y.C., Ko,T.P., Su,W.C., Su,T.L. and Wang,A.H. (2009) Terpyridine-platinum(II) complexes are effective inhibitors of mammalian topoisomerases and human thioredoxin reductase 1. *J. Inorg. Biochem.*, **103**, 1082–1092.
20. Ahmadi,R., Urig,S., Hartmann,M., Helmke,B.M., Koncarevic,S., Allenberger,B., Kienhoefer,C., Neher,M., Steiner,H.H., Unterberg,A. *et al.* (2006) Antiglioma activity of 2,2′:6′, 2″-terpyridineplatinum(II) complexes in a rat model—effects on cellular redox metabolism. *Free Radic. Biol. Med.*, **40**, 763–778.
21. Witte,A.B., Anestål,K., Jerremalm,E., Ehrsson,H. and Arnér,E.S. (2005) Inhibition of thioredoxin reductase but not of glutathione reductase by the major classes of alkylating and platinum-containing anticancer compounds. *Free Radic. Biol. Med.*, **39**, 696–703.
22. Becker,K., Herold-Mende,C., Park,J.J., Lowe,G. and Schirmer,R.H. (2001) Human thioredoxin reductase is efficiently inhibited by (2,2′:6′,2″-terpyridine)platinum(II) complexes. Possible implications for a novel antitumor strategy. *J. Med. Chem.*, **44**, 2784–2792.
23. Reedijk,J. (2003) New clues for platinum antitumor chemistry: kinetically controlled metal binding to DNA. *Proc. Natl Acad. Sci. USA*, **100**, 3611–3616.
24. Wheate,N.J. and Collins,J.G. (2003) Multi-nuclear platinum complexes as anti-cancer drugs. *Coord. Chem. Rev.*, **241**, 133–145.
25. Cox,J.W., Berners-Price,S.J., Davies,M.S., Qu,Y. and Farrell,N. (2001) Kinetic analysis of the stepwise formation of a long-range DNA interstrand cross-link by a dinuclear platinum antitumor complex: evidence for aquated intermediates and formation of both kinetically and thermodynamically controlled conformers. *J. Am. Soc. Chem.*, **123**, 1316–1326.
26. Lowe,G., Droz,A.S., Vilaivan,T., Weaver,G.W., Tweedale,L., Pratt,J.M., Rock,P., Yardley,V. and Croft,S.L. (1999) Cytotoxicity of (2,2′:6′,2″-Terpyridine)platinum(II) Complexes to Leishmania donovani, Trypanosoma cruzi, and Trypanosoma brucei. *J. Med. Chem.*, **42**, 999–1006.
27. Komeda,S., Lutz,M., Spek,A.L., Yamanaka,Y., Sato,T., Chikuma,M. and Reedijk,J. (2002) A novel isomerization on interaction of antitumor-active azole-bridged dinuclear platinum(II) complexes with 9-ethylguanine. platinum(II) atom migration from N2 to N3 on 1,2,3-triazole. *J. Am. Soc. Chem.*, **124**, 4738–4746.
28. Oehlsen,M.E., Qu,Y. and Farrell,N. (2003) Reaction of polynuclear platinum antitumor compounds with reduced glutathione studied by multinuclear (^{1}H, ^{1}H-^{15}N gradient heteronuclear single-quantum coherence, and ^{195}Pt) NMR spectroscopy. *Inorg. Chem.*, **42**, 5498–5506.
29. Weissm,R.B. and Christian,M.C. (1993) New cisplatin analogue in development. *Drugs*, **46**, 360–373.
30. Lamers,M.H., Perrakis,A., Enzlin,J.H., Winterwerp,H.H.K., Wind,N.D. and Sixma,T.K. (2000) The crystal structure of DNA mismatch repair protein MutS binding to a G.T mismatch. *Nature*, **407**, 711–717.
31. Obmolova,G., Ban,C., Hsieh,P. and Yang,W. (2000) Crystal structures of mismatch repair protein MutS and its complex with a substrate DNA. *Nature*, **407**, 703–711.
32. Jodrell,D.I., Evans,T.R.J., Steward,W., Cameron,D., Prendiville,J., Aschele,C., Noberasco,C., Lind,M., Carmichael,J., Dobbs,N. *et al.* (2004) Phase II studies of BBR3464, a novel tri-nuclear platinum

complex, in patients with gastric or gastro-oesophageal adenocarcinoma. *Eur. J. Cancer*, **40**, 1872–1877.

33. Jansen,B.A.J., Zwan,J.v.d., Reedijk,J., Dulk,H.d. and Brouwer,J. (1999) A tetranuclear platinum compound designed to overcome cisplatin resistance. *Eur. J. Inorg. Chem.*, **9**, 1429–1433.

34. Farrell,N. (2000) In Kelland,L.R. and Farrell,N.P. (eds), *Platinum-Based Drugs in Cancer Therapy*. Humana Press Inc., Totowa, New Jersey.

35. Brabec,V., Kasparkova,J., Vrana,O., Novakova,O., Cox,J.W., Qu,Y. and Farrell,N. (1999) DNA modifications by a novel bifunctional trinuclear platinum phase I anticancer agent. *Biochemistry*, **38**, 6781–6790.

36. Qu,Y., Farrell,N., Kasparkova,J. and Brabec,V. (1997) DNA binding of properties of trinuclear platinum complex. *J. Inorg. Chem.*, **67**, 174.

37. Roberts,J.D., Peroutka,J. and Farrell,N. (1999) Cellular pharmacology of polynuclear platinum anti-cancer agents. *J. Inorg. Biochem.*, **77**, 51–57.

38. Zhao,Y., He,W., Shi,P., Zhu,J., Qiu,L., Lin,L. and Guo,Z. (2006) A positively charged trinuclear 3N-chelated monofunctional platinum complex with high DNA affinity and potent cytotoxicity. *Dalton Trans.*, 2617–2619.

39. Zhu,J., Zhao,Y., Zhu,Y., Wu,Z., Lin,M., He,W., Wang,Y., Chen,G., Dong,L., Zhang,J. *et al.* (2009) DNA cross-linking patterns induced by an antitumor active trinuclear platinum complex and comparison with its dinuclear analogue. *Chem. Eur. J.*, **15**, 5245–5253.

40. Chaney,S.G., Campbell,S.L., Bassett,E. and Wu,Y. (2005) Recognition and processing of cisplatin- and oxaliplatin-DNA adducts. *Crit. Rev. Oncol. Hematol.*, **53**, 3–11.

41. Sharma,S., Gong,P., Temple,B., Bhattacharyya,D., Dokholyan,N.V. and Chaney,S.G. (2007) Molecular dynamic simulations of cisplatin- and oxaliplatin-d(GG) Intrastand cross-links reveal differences in their conformational dynamics. *J. Mol. Biol.*, **373**, 1123–1140.

42. Merajver,S.D., Pham,T.M., Caduff,R.F., Chen,M., Poy,E.L., Cooney,K.A., Weber,B.L. and Frank,T.S. (1995) Somatic mutations in the BRCA1 gene in sporadic ovarian tumours. *Nat. Genet.*, **9**, 439–443.

43. Yang,X.-L. and Wang,A.H.-J. (1999) Structural studies of atom-specific anticancer drugs acting on DNA. *Pharmacol. Ther.*, **83**, 181–215.

44. Roothan,C.C.J. (1951) New developments in molecular orbital theory. *Rev. Mod. Phys.*, **23**, 69–89.

45. Pople,J.A. and Nesbet,R.K. (1954) Self-consistent orbitals for radicals. *J. Chem. Phys.*, **22**, 571–572.

46. McWeeny,R. and Diercksen,G. (1968) Self-consistent perturbation theory. II. Extension to open shells. *J. Chem. Phys.*, **49**, 4852–4856.

47. Frisch,M.J., Trucks,G.W., Schlegel,H.B., Scuseria,G.E., Robb,M.A., Cheeseman,J.R., J.A. Montgomery,J., Vreven,T., Kudin,K.N., Burant,J.C. *et al.* (2004) GUASSIAN 03, Revision D.01, Gaussian, Inc., Wallingford, CT.

48. Yao,S., Plastaras,J.P. and Marzilli,L.G. (1994) A molecular mechanics AMBER-type force field for modeling platinum complexes of guanine derivatives. *Inorg. Chem.*, **33**, 6061–6077.

49. Chval,Z. and Sip,M. (1998) Force field for platinum binding to adenine and guanine taking into account flexibility of nucleic acids bases. *J. Phys. Chem. B*, **102**, 1659–1661.

50. Cundari,T.R., Fu,W., Moody,E.W., Slavin,L.L., Snyder,L.A., Sommerer,S.O. and Klinckman,T.R. (1996) Molecular mechanics force field for platinum coordination complexes. *J. Phys. Chem.*, **100**, 18057–18064.

51. Case,D.A., Darden,T.A., Cheatham,I.T.E., Simmerling,C.L., Wang,J.M., Duke,R.E., Luo,R., Merz,K.M., Pearlman,D.A., Crowley,M. *et al.* (2006) *AMBER9*, University of California, San Francisco.

52. Lee,M.C. and Duan,Y. (2004) Distinguish protein decoys by using a scoring function based on a new AMBER force field, short molecular dynamics simulations, and the generalized born solvent model. *Proteins Struct. Funct. Bioinform.*, **55**, 620–634.

53. Wang,J.M., Wolf,R.M., Caldwell,J.W., Kollamn,P.A. and Case,D.A. (2004) Development and testing of a general Amber force field. *J. Comput. Chem.*, **25**, 1157–1174.

54. Miyamoto,S. and Kollman,P.A. (1992) Settle: an analytical version of the SHAKE and RATTLE algorithm for rigid water models. *J. Comput. Chem.*, **13**, 952–962.

55. Lavery,R. and Sklenar,H. (1988) The definition of generalized helicoidal parameters and of axis curvature for irregular nucleic acids. *J. Biol. Struct. Dyn.*, **6**, 63–91.

56. Strahs,D. and Schlick,T. (2000) A-tract bending: insights into experimental structures by computational models. *J. Mol. Biol.*, **301**, 643–663.

57. Amadei,A., Linssen,A.B., Groot,B.L.D., Aalten,D.M.V. and Berendsen,H.J. (1996) An efficient method for sampling the essential subspace of proteins. *J. Biomol. Struct. Dyn.*, **13**, 615–623.

58. Amadei,A., Linssen,A.B.M. and Berendsen,H.J.C. (1993) Essential dynamics of proteins. *Proteins: Structure, Function, and Genetics*, **17**, 412–425.

59. Yamaguchi,H., Aalten,D.M.V., Pinak,M., Furukawa,A. and Osman,R. (1998) Essential dynamics of DNA containing a cis.syn cyclobutane thymine dimer lesion. *Nucleic Acids Res.*, **26**, 1939–1946.

60. Teeter,M.M. and Case.,D.A. (1990) Harmonic and quasiharmonic descriptions of crambin. *J. Phys. Chem.*, **94**, 8091–8097.

61. van Aalten,D.M., Findlay,J.B., Amadei,A. and Berendsen,H.J. (1995) Essential dynamics of the cellular retinol-binding protein–evidence for ligand-induced conformational changes. *Protein Eng.*, **8**, 1129–1135.

62. Yang,D., Boom,S.S.G.E.v., Reedijk,J., Boom,J.H.V. and Wang,A.H.-J. (1995) Structure and isomerization of an intrastrand cisplatin-cross-linked octamer DNA duplex by NMR analysis. *Biochemistry*, **34**, 12912–12920.

63. Spingler,B., Whittington,D.A. and Lippard,S.J. (2001) 2.4 Å crystal structure of an oxaliplatin 1,2-d(GpG) intrastrand cross-link in a DNA dodecamer duplex. *Inorg. Chem.*, **40**, 5596–5602.

64. Marzilli,L.G., Saad,J.S., Kuklenyik,Z., Keating,K.A. and Xu,Y. (2001) Relationship of solution and protein-bound structures of DNA duplexes with the major intrastrand cross-link lesions formed on cisplatin binding to DNA. *J. Am. Soc. Chem.*, **123**, 2764–2770.

65. Takahara,P.M., Frederick,C.A. and Lippard,S.J. (1996) Crystal structure of the anticancer drug cisplatin bound to duplex DNA. *J. Am. Soc. Chem.*, **118**, 12309–12321.

66. Tzou,W.S. and Hwang,M.J. (1999) Modeling helix-turn-helix protein-induced DNA bending with knowledge-based distance restraints. *Biophys. J.*, **77**, 1191–1205.

67. Neidle,S. (1994) *DNA Structure and Recognition*. Oxford University Press, Oxford.

68. Abu-Surrah,A.S. and Kettunen,M. (2006) Platinum group antitumor chemistry: design and development of new anticancer drugs complementary to cisplatin. *Curr. Med. Chem.*, **13**, 1337–1357.